Towards the generation of broadband optical vortices: extending the spectral range of a q-plate by polarization-selective filtering

MINDAUGAS GECEVICIUS[1,3], MAKSYM IVANOV[2], MARTYNAS BERESNA[1], AIDAS MATIJOSIUS[2*], VIKTORIJA TAMULIENE[2], TITAS GERTUS[4], AUSRA CERKAUSKAITE[1], KIPRAS REDECKAS[2], MIKAS VENGRIS[2], VALERIJUS SMILGEVICIUS[2], AND PETER G. KAZANSKY[1]

[1] *Optoelectronics Research Centre, University of Southampton, SO17 1BJ, Southampton, United Kingdom*
[2] *Vilnius University Laser Research Center, 10 Sauletekio avenue, LT- 10223, Vilnius, Lithuania*
[3] *State Key Laboratory of Luminescent Materials and Devices, South China, University of Technology, Guangzhou 510640, China*
[4] *Altechna R&D Ltd., Mokslininku st. 6A, LT-08412, Vilnius, Lithuania*
[*] *Corresponding author: aidas.matijosius@ff.vu.lt*

Compiled November 24, 2017

Optical vortex beams in the visible and nIR spectrum over a wide spectral region are generated by a single S-Waveplate polarization converter using polarization-selective filtering. A spectral coverage of 600 nm is demonstrated, with maximum efficiency at a wavelength of 530 nm. The broadband coverage is obtained using polarization filtering, which is applicable for any component based on geometric phase retardation. The efficiency of the filtering varies from 50% to 95% depending on the wavelength. This technique has a potential application in stimulated emission depletion (STED) microscopy and lithography.

OCIS codes: (050.4865) Optical vortices; (230.5440) Polarization-selective devices.

http://dx.doi.org/10.1364/ao.XX.XXXXXX

1. INTRODUCTION

Optical orbital angular momentum (OAM) of $l\hbar$ per photon ($\hbar$ is the reduced Planck constant) [1] rises in the light fields with screw wavefront dislocations [2]. Phase of these beams varies azimuthally and their complex amplitude is proportional to $e^{il\phi}$, where l is referred to as topological charge, r and ϕ are the radius and azimuthal angle, respectively. Such OAM beams are frequently referred to as Optical Vortices (OVs) [3]. Due to the presence of OAM and doughnut shaped intensity distribution OVs have found applications in various areas [4–9]. In most of those applications broadband or at least widely tunable OVs are desired; however, their generation is technically challenging due to inherent dependence on wavelength λ. Indeed, the wavefront of OVs which give rise of OAM has the tilt of $l\lambda/2\pi r$ [10].

An exotic method of broadband OV generation exploits nonlinear processes [11]. However, the simpler (hence more practical) techniques rely on amplitude, phase and/or polarization modulation of a Gaussian beam in a dedicated optical component. The most common component is a forked hologram recorded on photographic film [12] or displayed with spatial light modulator [13] that modulates amplitude or phase of an initial beam. Due to the diffractive nature of such modulation, this technique suffers from chromatic angular dispersion [14] and requires compensation schemes. The widest OV bandwidth demonstrated to date used a forked grating inscribed in a phase hologram and covered 250 nm range with the central wavelength of $\lambda_0 = 800$ nm [15].

Phase plates with varying azimuthal thickness can generate OVs over 140 nm range in the visible [16]. Their bandwidth depends on the phase plate material.

Polarization-based methods include axially-symmetric polarizer [17], quarter [18] and half [19] waveplates, and a glass cone [20]. These methods can theoretically produce OVs in the entire visible spectrum, however, they lack sufficient spatial resolution in the axial part of the component, which is essential in applications such as stellar coronagraphy [21]. Additionally, the methods described in [19, 20] are limited to $|l|$=2. Due to dispersive nature of glass, OV generated with the glass cone [20] exhibits spatial and chromatic dispersions. Separately, polarization grating [22] should be mentioned. It provides extremely high efficiency over wide spectral region, however, suffers chromatic dispersion and has a relatively low damage threshold of liquid crystals.

Recognition of eigenmodes of light in the form of Laguerre-Gaussian (LG) modes in a homogeneous anisotropic medium

(e.g. uniaxial crystals) [23], created a wave of subsequent studies of broadband OVs generation from spin-orbit coupling of angular momentum (AM) of light in uniaxial and biaxial crystals. Biaxial crystals demonstrated bandwidth of 250 nm after additional compensation of chromatic dispersion [24]. Uniaxial crystals demonstrated 360 nm bandwidth (but are not limited to this value) [25–27]. To generate OV, Gaussian beam should be focused onto the crystal. The radial index of the generated LG mode depends on the angle of divergence of the initial beam and crystal length. Q-plate is another class of components that uses spin-to-orbit coupling of AM. Q-plate is a spatially variant half-wave plate, which by changing polarization of the incident beam changes its geometric (Pancharatnam-Berry) phase [28]. When slow (fast) optical axis spatially varies in the form of $\psi = q\phi$ (with q half-integer) and birefringent phase retardation is π (half-wave) then the AM of light is not transferred to the material but directly converts from spin to orbital. Three most common techniques of inducing π phase retardation are based on liquid crystals (LC), photonic crystals (PC) and nano-gratings (sub-wavelength gratings). LC based q-plates allow tuning of a plate to a certain wavelength by changing the applied voltage [29, 30], but do not allow simultaneous coverage of a broad spectrum range. PC based q-plates demonstrate 300 nm bandwidth (from 500 to 800 nm) [31]. Nano-grating (sub-wavelength grating) based q-plates are also referred to as super-structured wave plates (S-waveplates). The period of spatial structures in such plates is shorter than the wavelength of light in the visible spectrum [32–34]. These components exhibit high spatial resolution of patterning in the axial area and are resistant to optical damage [35]. However, their specified bandwidth is 20 nm around the central wavelength.

A decade ago, it was suggested that additional polarization sensitive [36] or spatial filtering [37] can significantly broaden the spectral performance of Pancharatnam-Berry phase elements. However, the experimental efforts were confined to far-infrared spectral range and did not demonstrate the polarization sensitive beam cleaning as spatial filtering was performed instead [37]. Similar polarization filtering was performed to reduce dispersion of topological charge of high order OVs [38] (without theoretical description of the process). Yet, enhancement of spectral performance was not demonstrated.

In this article, using proposed polarization-sensitive filtering, we demonstrate generation of an optical vortex beam over the entire visible and near infrared range, from temporarily coherent and incoherent light sources. This technique allows converting any wavelength dependent (chromatic) Pancharatnam-Berry phase element to an achromatic one. We have employed a high damage threshold S-waveplate with an initial bandwidth of 20 nm (around the central wavelength of 532 nm) and demonstrated that it can be used to generate high contrast OV beams at any given wavelength in the range between 400 nm and 1040 nm. The efficiency of the filtering and possible applications of this technique are discussed.

2. OPTICAL VORTICES OVER OCTAVE-SPANNING SPECTRAL RANGE

A. Theory

Although topological charge l of the S-waveplate could reach higher values [39], in the following we restrict our considerations to $l = 1$. The S-Waveplate acts as a half-wave plate phase retarder and it's operation can be described by the Jones matrix formalism. The matrix for the S waveplate is as follows:

$$M_s = \begin{bmatrix} \cos(2\theta) & \sin(2\theta) \\ \sin(2\theta) & -\cos(2\theta) \end{bmatrix}; \quad (1)$$

where θ is an azimuthal angle of the optical axis of a half-wave plate. The resulting light field E_{out} can be presented as an action of a half-wave plate converter M_S on the initial field E_{in}: $E_{out} = M_s E_{in}$. If a right-handed circularly polarized light is transmitted through the S-Waveplate, a left-handed circularly polarized OV (with the topological charge equal to 1) is generated:

$$E_{out} = \frac{1}{\sqrt{2}} M_s \begin{bmatrix} 1 \\ i \end{bmatrix} E_{in} = \frac{1}{\sqrt{2}} e^{i2\theta} \begin{bmatrix} 1 \\ -i \end{bmatrix} E_{in}, \quad (2)$$

where $E_{in} = e^{-r^2/w^2} e^{-i(2\pi/\lambda_0)r^2/(2R')}$ is Gaussian envelope, $R' = z(1 + (z'/z)^2)$, $z' = \pi w_0^2/\lambda$, $r^2 = x^2 + y^2$, x, y and z are Cartesian coordinates, w is waist of the beam and λ is the wavelength of light. So, left (right) handed circularly polarized light passed S-waveplate acquires vortex phase and orthogonal right(left) handed circular polarization. However, if the wavelength of incident light, λ, differs from the wavelength the S-waveplate was designed for, λ_0, the value of phase retardation would be different for different wavelengths: $\Delta = \pi\lambda_0/\lambda$. It means that only light at the wavelength λ_0 would remain circularly polarized. Arbitrary wavelength λ would acquire elliptical polarization and phase retardation Δ. By multiplying Jones vector for left circular polarization with Jones matrix for the retarder (S-waveplate) with phase retardation Δ and azimuth θ (orientation of optical axis), we can calculate how circular polarization of the input light will be transformed:

$$E_{el} = \frac{1}{\sqrt{2}} \begin{bmatrix} cos^2(\theta) + e^{i\Delta} sin^2(\theta) & (1 - e^{i\Delta}) sin(\theta) cos(\theta) \\ (1 - e^{i\Delta}) sin(\theta) cos(\theta) & sin^2(\theta) + e^{i\Delta} cos^2(\theta) \end{bmatrix} \begin{bmatrix} 1 \\ i \end{bmatrix} E_{in} = \frac{1}{\sqrt{2}} \begin{bmatrix} cos^2(\theta) + e^{i\Delta} sin^2(\theta) + i(1 - e^{i\Delta}) sin(\theta) cos(\theta) \\ (1 - e^{i\Delta}) sin(\theta) cos(\theta) + i(sin^2(\theta) + e^{i\Delta} cos^2(\theta)) \end{bmatrix} E_{in} \quad (3)$$

Eq. 3 does not give much information on phase or polarization dependence of the beam on phase retardation Δ or azimuthal angle θ. Now let us assume that the light with such polarization E_{el} (Eq. 3) passes the left L or right R circular polarizer (quarter wave plate and linear polarizer). Then, the electric fields (E_R and E_L) will be following:

$$E_{right} = RE_{el} = \frac{1}{2\sqrt{2}} (1 - e^{i\Delta}) e^{i2\theta} \begin{bmatrix} 1 \\ -i \end{bmatrix} E_{in}; \quad E_{left} = LE_{el} = \frac{1}{2\sqrt{2}} (1 + e^{i\Delta}) \begin{bmatrix} 1 \\ i \end{bmatrix} E_{in}, \quad (4)$$

where R and L are the Jones matrices for right and left circular polarizers, respectively:

$$R = \frac{1}{2} \begin{bmatrix} 1 & i \\ -i & 1 \end{bmatrix}; L = \frac{1}{2} \begin{bmatrix} 1 & -i \\ i & 1 \end{bmatrix}; \quad (5)$$

After the left-handed circularly polarized light of $\lambda \neq \lambda_0$ passes through the S-waveplate and a right-handed circular polarizer, the electric field E_R (Eq. 4) becomes similar to what

we would expect after passing through the S-waveplate when $\lambda = \lambda_0$ (Eq. 2). It contains the same factor $e^{i2\theta}$ which indicates the azimuthal phase variation of the field, i.e. presence of an OV. However, after the left-handed circular polarizer, the electric field E_L (Eq. 4) does not have this azimuthally dependent term. Therefore, after the S-waveplate, the circularly polarized light of wavelength $\lambda \neq \lambda_0$ can be separated into two parts according to the handedness of polarization. Only one of the polarizations will exhibit the azimuthally varying phase dependence, i.e. become an OV.

The ratio of the two resultant fields depends only on the phase retardation of the retarder:

$$I_R = E_{Rx}E^*_{Rx} + E_{Ry}E^*_{Ry} = \frac{1}{2}(1 - \cos \pi\lambda_0/\lambda) \quad \textbf{(6)}$$

$$I_L = E_{Lx}E^*_{Lx} + E_{Ly}E^*_{Ly} = \frac{1}{2}(1 + \cos \pi\lambda_0/\lambda) \quad \textbf{(7)}$$

In summary, even if any S-Waveplate or, in general, any other optical element based on the phase control of circularly polarized light by half-wave plates (e.g. [40]) is designed for a specific wavelength, a desired transformed part of the beam can be easily separated out using a circular polarizer.

As an illustration, using previous equations 4 and a Fourier propagation method, a situation was simulated, where a circularly polarized beam passes through the S-Waveplate, quarter-wave plate and a linear polarizer (Fig. 1). The modelled S-Waveplate is set for $\lambda_0 = 530$ nm wavelength, whereas the spectrum of the incident light ranges from 400 nm to 1000 nm. The results indicate that the contrast of the vortex beam generated with the S-Waveplate strongly depends on the wavelength (Fig. 1 (ii)). However, after passing the circular polarizer, at all wavelengths a high contrast OV is obtained (Fig. 1 (iii)), with zero intensity at the center. Due to the wavelength mismatch all the "background", i.e. not phase modulated part of the beam is separated to the orthogonally polarized field (Fig. 1 (iv)).

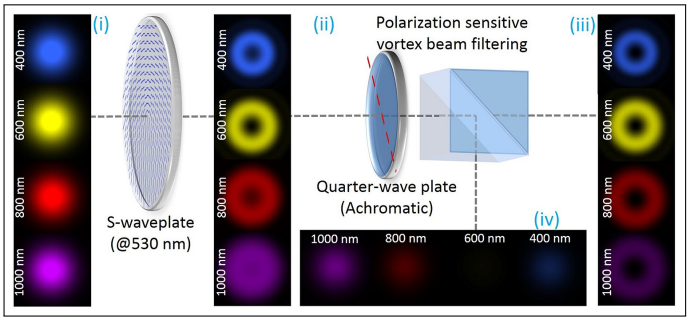

Fig. 1. The simplified schematic and numerical model for OVs generation and polarization-sensitive beam cleaning. Gaussian beams (i) pass through the S-Waveplate, resulting in OVs with different contrast, depending on the wavelength (ii). The quarter-wave plate and linear polarizer work as a polarization-sensitive vortex beam filter that separates the vortex beam (iii) and the background with no phase modulation (iv).

B. Experiment

We used an S-Waveplate designed for 530 nm (fabricated by Altechna R&D, developed at the University of Southampton [32, 33]). The S-Waveplate was illuminated with femtosecond light pulses tuned in the range of $400 - 1040$ nm from an optical parametric amplifier "Topas" (Light Conversion Ltd.). The experimental setup was similar to the one illustrated in the Fig. 1. However, to achieve a perfect achromatic behaviour in a wide spectral range, achromatic quarter-wave plates (for circular polarization generation and for circular analyser) were replaced with two Fresnel rhombs and a calcite crystal was used to separate two orthogonal polarizations. The beam profiles were measured using a CCD camera (Chameleon CMLN-13S2M-CS).

C. Results and discussion

The contrast (intensity in the center of the beam divided by the maximum intensity of the beam: I_{min}/I_{max}) of the OVs generated by the S-Waveplate strongly depended on the wavelength (Fig. 2 (ii)). At wavelengths close to the design wavelength of 530 nm, the generated beams exhibited a well-defined doughnut shape, while at nearly twice longer wavelength ($\sim$ 1000 nm) the generated beam had a flat top profile with no sign of singularity at the center. However, after the polarization-sensitive beam cleaning part of the setup (second Fresnel rhomb and calcite crystal), vortex and Gaussian parts of the beams were separated into two beams (Fig. 2 (iii,iv)).

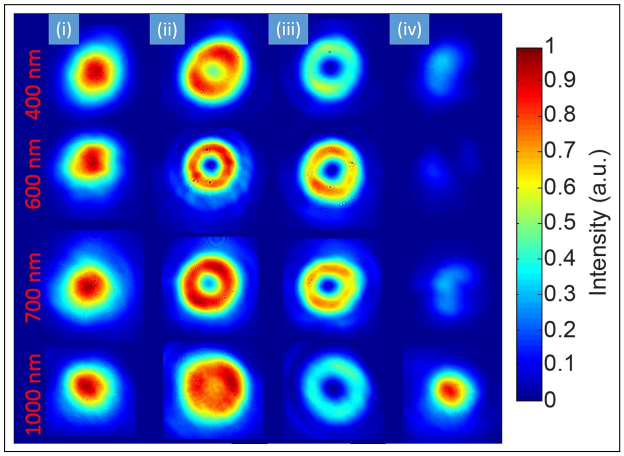

Fig. 2. Experimental intensity distributions of: (i) Initial Gaussian beam before S-Waveplate; (ii) – beam after S-Waveplate; (iii) filtered vortex part of the beam (after a quarter-wave plate and a linear polarizer); (iv) Gaussian (background) part of the beam (after quarter-wave plate and linear polarizer).

The further analysis of beams presented in Fig. 2 (ii,iii) and (iii,iv) is shown in Fig. 3 and 4, respectively. The performance of the polarization-sensitive beam cleaning was evaluated by comparing the contrast of the generated OVs before and after beam cleaning (Fig. 3 (a)). Before beam cleaning, the contrast exhibit a strong dependence on wavelength, whilst after the cleaning, contrast of OV is similar at all wavelengths. Small variations in the contrast after cleaning is caused by the variations in the quality of the input Gaussian beam (Fig. 2 (i)) rather than the chromaticity of the setup.

In order to confirm the presence of phase helicity in the vortex part of the beam and its absence in the orthogonally polarized part, both parts of the beams were injected into a Michelson interferometer and interference patterns were measured (Fig. 3 (b)). As predicted, the interference pattern of the vortex beam exhibited a forked structure (which is a clear indication of the phase helicity) whereas the orthogonally polarized Gaussian (background) part of the beam produced regular fringes.

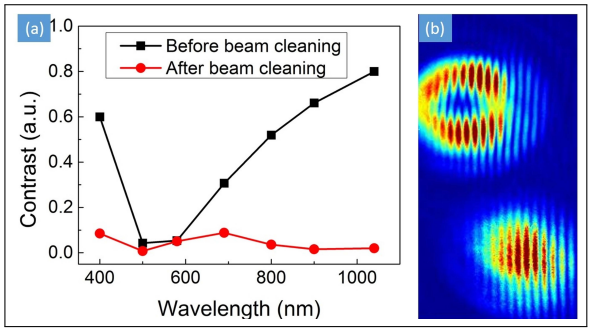

Fig. 3. (a) The contrast of generated vortex beams at different wavelength before and after the polarization sensitive beam cleaning. (b) Interference of vortex- and Gaussian part (background) of the beam (at 1000 nm).

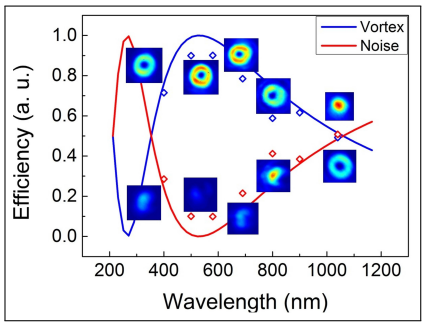

Fig. 4. Polarization sensitive beam cleaning efficiency dependence on the wavelength. Experimental points are compared with the theoretical curve. Insets demonstrate measured beam profiles of generated OVs and beams profiles of filtered out background at different wavelengths.

The reason for one polarization component to acquire vortex structure and for other not to is following. The beam is being transformed to OV by acquiring phase retardation $\lambda_0/2$ and changing its polarization state to orthogonally polarized. When the incident wavelength $\lambda \neq \lambda_0$, the phase delay and polarization state depend on λ; the beam become elliptically polarized. Dividing the beam into two orthogonally polarized parts and selecting the polarization orthogonal to initial, we automatically select the light which acquired $\lambda_0/2$ phase delay. Therefore, one polarization component carry an OV and other does not.

Fig. 2 (iii,iv) shows that unlike the contrast, the power ratio between the cleaned vortex part of the beam and not phase modulated background (Gaussian "noise") part strongly depends on wavelength. The efficiency of the vortex/Gaussian conversion at different wavelengths (Fig. 4) can be evaluated using Eq. 7. Maximum efficiency is achieved at the design wavelength of the S-Waveplate; the efficiency remains above 50% at the wavelength nearly two times larger than the design wavelength, demonstrating successful OV generation in the 600 nm wavelength range (in this range, the efficiency is more than 50%). Obviously the bandwidth scales with the central wavelength: an S-Waveplate designed for the 1 μm wavelength would cover the bandwidth of 1.2 μm.

Besides OVs generation in a broad wavelength range, the presented scheme can also work as a polarization selective vortex converter. The handedness of circular polarization determines whether the Gaussian beam passing through the setup stays Gaussian or is converted to an OV. Therefore, for example, if we have two beams with different wavelengths and orthogonal circular polarizations, only one of them will be converted to a vortex beam and the other would remain unaffected (Fig. 5 (a)). This could be useful for stimulated emission depletion (STED) applications as both beams could travel in the same optical path and just before the objective, one of them would be converted to a vortex beam. The advantage of such geometry has already been demonstrated in [6, 41], where an OV was generated using a highly chromatic optical component, which imposed a limit on how close the two wavelengths could be. Since our method is based on polarization selection, there is no such wavelength limitation for the two beams; only the "correctly" polarized beam will be converted to a vortex. In order to demonstrate how this works in practice, we performed an experiment using the setup illustrated in Fig. 5 (a). We used three lasers with different wavelengths: red – HeNe laser (633 nm), green – second harmonics of Nd:YAG laser (532 nm), blue – OPA output at 400 nm wavelength. Orthogonally polarized beams of two of the lasers (red and green or blue and green) were launched collinearly through the polarization sensitive OV generator. As shown in Fig. 5 (b), in each case, only one beam (green in the presented case) was transformed into a vortex whereas the other remained Gaussian. With currently available laser sources intensity efficiency of the methods does not impose limitation for the application. The proposed scheme with single optical path for both excitation and depletion beams could significantly facilitate extremely complicated process of alignment of STED systems.

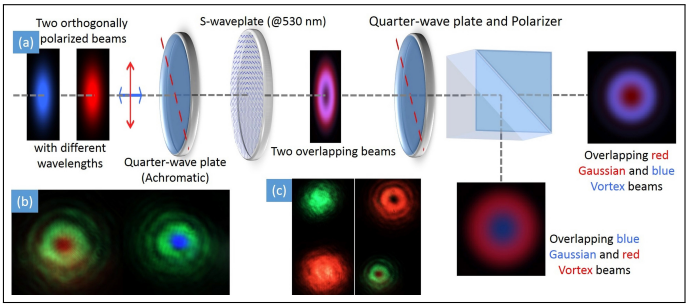

Fig. 5. Polarization selective vortex beam generation: (a) experimental set-up and modeled results; (b) experimentally measured profiles of green (532 nm) vortex beam after polarization transformation superimposed with orthogonally polarized red (633 nm) and blue (400 nm) Gaussian beams in the middle; (c) experimental beam profiles (532 nm and 633 nm) before (on the left) and after (on the right) polarization sensitive transformation.

3. OPTICAL VORTEX GENERATED FROM AN INCOHERENT WHITE LIGHT SOURCE

A. Theory

In this section, we expand our previous considerations to generate "white" light OV. Hereafter, white light means a broadband incoherent light emitted by an incandescent halogen lamp. Temporally incoherent incident light field $A(t)$ is given by the Gaussian-Gaussian noise model [42]:

$$A(t) = \frac{1}{\sqrt{N}} \sum_{j=1}^{N} e^{(it\Omega_j + i\xi_j)}, \quad (8)$$

where $\Omega_j = \omega_j - \omega_0$, ω_0 and ω_j are the central and normally distributed random frequencies, respectfully; dispersion σ^2 ($\sigma = (\omega_1 - \omega_2)/2\sqrt{2}$, $\omega_{1,2} = 2\pi c/\lambda_{1,2}$, c – speed of light). ξ_j are uniformly distributed random phases. N has to be significantly large in the simulation (here $N = 471$). The wavelengths $\lambda_1 =$ 360 nm and $\lambda_2 = 830$ nm, $\lambda_0 = 530$ nm. Intensity distributions after each component in the experimental setup are obtained by the multiplication of the Fourier transformed complex amplitude $A(t)$ by the Jones matrix of the corresponding optical element. For example, the vortex E_V and not phase modulated E_G parts of the beam after the polarization filtering are given by:

$$E_{V(G)} = E_{right(left)} S(\omega), \tag{9}$$

where $S(\omega)$ is the Fourier transform of the $A(t)$, $E_{right(left)}$ is given by Eq. 4. Such field has Gaussian shaped spectrum and obeys Gaussian statistics [42]. Modeled intensity distributions are shown in the top row of the Fig. 7.

B. Experiment

For the white-light experiment the light source in the experimental setup described in the section 3B was substituted by a 55 W tungsten halogen bulb and used as the source of an incoherent broadband white light. The light from the halogen bulb was collected (without focusing system) by a multimode gradient optical fiber (86 cm long, cladding diameter 850 μm, core diameter 130 μm) placed close to the lamp. Only the light propagating through the core of the fiber was then selected by the first aperture (diameter 0.95 mm) placed 21 mm after the tip of the fiber. The spatial coherence of the light was controlled by the size of this aperture. It should be small enough to provide sufficient degree of spatial coherence for the generated optical vortex to be visible, i.e. to posses deep axial minimum of intensity ([26, 43] and references within). "White"-light beam with a high degree of spatial coherence was then collimated with the aid of a pair of lenses in the telescope configuration and spatially filtered by the second aperture (diameter 110 μm) placed in the common focus between these lenses. The role of the second aperture was to endow the beam with nearly Gaussian intensity profile and to control its waist size. The polarization tailoring of the beam were achieved by Fresnel rhombs and a Glan polarizer. An angle cut calcite crystal was used to separate two polarization states. Colored images of the beam were obtained by Canon 600d camera with the default settings for the white balance, saturation, contrast and color tone.

C. Results and discussion

Bandwidth of the incident white light spans from 325 nm to 1030 nm and is shown in the Fig. 6a (solid black curve marked as "Initial experimental"). However, for modeled intensity distributions spectrum in the limits of human eye perception was used: from 360-830 nm (hollow brown circles in the Fig. 6a). The "white" light beam acquired its vortex structure upon propagation through the S-waveplate designed for conversion of light in the 20 nm bandwidth (as stated by the manufacturer) around its central wavelength of 532 nm. Due to the far exceeding bandwidth of the incident "white" light, the visibility of the vortex core (zero intensity at the axis) is "masked" in the beam right after the S-waveplate (Fig. 7). As described in the previous sections, the maximum conversion efficiency is around design wavelength of the S-waveplate. Hence, the central part of the beam right after the S-waveplate is filled by the pink-violet shades, which are result of the substruction of green shades from

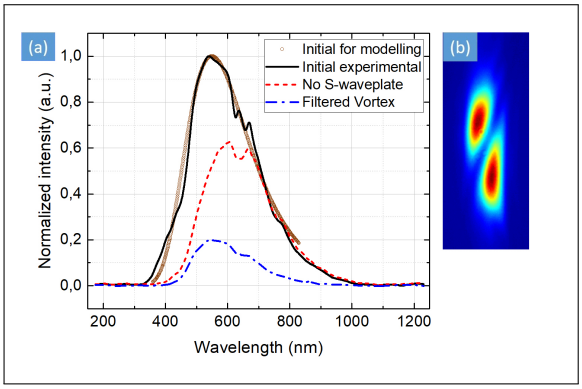

Fig. 6. (a) Spectra of the "white" light beam in different states. *Experimental*: Black (solid): initial unpolarized white light; Red (dashed): spectrum of the polarized collimated beam after passing all the polarization optics but the S-waveplate; Blue (dashed-doted): vortex part of the beam after the polarization filtering (i.e. beam passed all the polarization optics and the S-waveplate). *Modeled*: Brown (hollow circles): initial spectrum used for modeling; cut at the limits of visible light. (b) Generated "white" light OV focused by a cylindrical lens. See text for details.

the white color. After the polarization selective filtering vertically polarized part of the beam with "clean" vortex structure (zero axial intensity) is spatially separated from the horizontally polarized background part of the beam having no phase singularity. Intensity normalized experimental images are shown in the Fig. 7 bottom row and demonstrate good agreement with the model. Outer red shades and inner blue shades of the circle of light of OV could be explained by the scattering of white light on objects smaller then the wavelength of light, which are the nano "cracks" the grating of the S-waveplate is made of.

The spectrum of the filtered optical vortex is shown in the Fig. 6a marked as "Filtered vortex" (dashed-dotted blue curve). Red dashed curve in the Fig. 6a marked as "No S-waveplate" shows spectrum of the beam after it passed through all the polarizing optics in the setup (under condition that the S-waveplate is removed from the setup). Because some of the polarizing elements were made from calcite, the spectrum of the beam was cut at the blue side, so it differs from initial and spans from 400 to 1000 nm. The spectrum of the filtered vortex has its maximum at 545 nm and spans from 410 to 900 nm. Conversion efficiency at different wavelengths differs as described in the previous sections.

Different frequency components acquire different phase delay, resulting in a topological charge dispersion [44]. Based on this effect vortex with half integer topological charge $|l| = 1/2$ can be generated when the S-waveplate is illuminated by twice the wavelength it is designed for [45]. Above described polarization filtering compensate topological charge dispersion resulting in equal TC for all spectral components [38]. To demonstrate unit topological charge of the generated "white" light OV $|l| = 1$ the beam after the polarization filtering was focused by a cylindrical lens (focal distance f = 125 mm) as described in [46]. At the focal area the light possessed one dark stripe across the intensity distribution (Fig. 6b) indicating that the value of topological charge is $|l| = 1$. OV generation occurs through the phase and polarization modulation. Thus, optical vortices at different frequency components demonstrate coaxiality, hence, avoid anomalous spectral behavior near the vortex core [47].

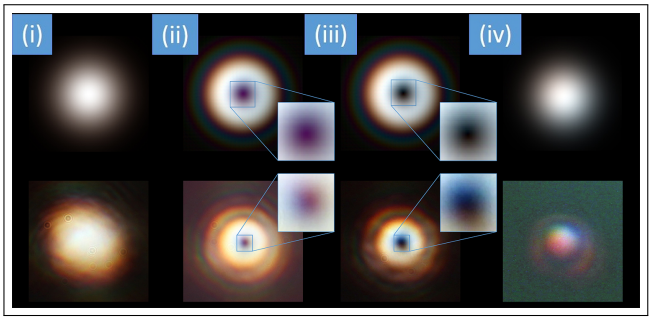

Fig. 7. Intensity normalized numerical plots (top row) and experimental images (bottom row) of the beam from incoherent light source in the states (i), (ii), (iii) and (iv) as described in the Figs. 1 and 2.

4. CONCLUSIONS

We have demonstrated generation of optical vortices over the visible and nIR wavelength range by using a single three-component scheme based on polarization-sensitive filtering. The filtering scheme consists of widely available components, is simple to implement and can be extended to any optical element based on the phase control of circularly polarized light, e.g. q-plates, not only as optical vortex converter but also as, e.g., Airy beam converter [40]. The demonstrated wavelength range spans over 600 nm over the VIS and nIR range with the efficiency of filtering higher than 50%. Due to the polarization modulation the presented scheme ensures coaxiality, no spatial dispersion of optical vortices generated at different wavelengths, which could be useful for generation of ultrashort OV shaped pulses in quantum communication systems and data transformation through photonic fibers. We have also demonstrated the polarization-selective vortex generation, where only one of two orthogonally polarized beams with different wavelengths is transformed to optical vortex (doughnut mode) with no limit on how close the two wavelengths could be. Proposed scheme with single optical path for both excitation and depletion beams could significantly facilitate extremely complicated process of alignment of STED systems.

M. Ivanov acknowledges financial support from the Erasmus Mundus Action 2 MID project.

REFERENCES

1. M. Padgett, J. Courtial, and L. Allen, "Light's orbital angular momentum," Phys. Today **57**, 35 (2004).
2. J. F. Nye and M. V. Berry, "Dislocations in wave trains," Proc. R. Soc. London A Math. Phys. Eng. Sci. **336**, 165–190 (1974).
3. P. Coullet, L. Gil, and F. Rocca, "Optical vortices," Opt. Commun. **73**, 403–408 (1989).
4. H. Huang, G. Xie, Y. Yan, N. Ahmed, Y. Ren, Y. Yue, D. Rogawski, M. J. Willner, B. I. Erkmen, K. M. Birnbaum, S. J. Dolinar, M. P. J. Lavery, M. J. Padgett, M. Tur, and A. E. Willner, "100 tbit/s free-space data link enabled by three-dimensional multiplexing of orbital angular momentum, polarization, and wavelength," Opt. Lett. **39**, 197–200 (2014).
5. M. P. J. Lavery, F. C. Speirits, S. M. Barnett, and M. J. Padgett, "Detection of a spinning object using light's orbital angular momentum," Science **341**, 537–540 (2013).
6. L. Yan, P. Gregg, E. Karimi, A. Rubano, L. Marrucci, R. Boyd, and S. Ramachandran, "Q-plate enabled spectrally diverse orbital-angular-momentum conversion for stimulated emission depletion microscopy," Optica **2**, 900–903 (2015).
7. J. Fischer and M. Wegener, "Three-dimensional optical laser lithography beyond the diffraction limit," Laser Photonics Rev. **7**, 22–44 (2012).
8. G. Foo, D. M. Palacios, , and J. G. A. Swartzlander, "Optical vortex coronagraph," Opt. Lett. **30**, 3308—-3310 (2005).
9. M. Geceviius, R. Drevinskas, M. Beresna, and P. G. Kazansky, "Single beam optical vortex tweezers with tunable orbital angular momentum," Appl. Phys. Lett. **104**, 231110 (2014).
10. J. Leach, S. Keen, C. S. Miles J. Padgett, , and G. D. Love, "Direct measurement of the skew angle of the poynting vector in a helically phased beam," Opt. Express **14**, 11919–11924 (2006).
11. S. Ramachandran, C. Smith, P. Kristensen, and P. Balling, "Nonlinear generation of broadband polarisation vortices," Opt. Express **18**, 23212–23217 (2010).
12. V. Y. Bazhenov, M. V. Vasnetsov, and M. S. Soskin, "Laser beams with screw dislocations in their wavefronts," Pis. Zh. Eksp. Teor. Fiz. (JETP Lett.) **52**, 1037—-1039(429—-432) (1990).
13. H. I. Sztul, V. Kartazayev, and R. R. Alfano, "Laguerre-gaussian supercontinuum," Opt. Lett. **31**, 2725–2727 (2006).
14. M. S. Soskin, P. V. Polyanskii, and O. O. Arkhelyuk, "Computer-synthesized hologram-based rainbow optical vortices," New J. Phys. **6**, 196 (2004).
15. J. Atencia, M.-V. Collados, M. Quintanilla, J. Marin-Saez, and I. J. Sola, "Holographic optical element to generate achromatic vortices," Opt. Express **21**, 21056–21061 (2013).
16. J. Grover A. Swartzlander, "Achromatic optical vortex lens," Opt. Lett. **31**, 2042–2044 (2006).
17. Y. Tokizane, K. Oka, and R. Morita, "Supercontinuum optical vortex pulse generation without spatial or topological-charge dispersion," Opt. Express **17**, 14519–14525 (2009).
18. T. Wakayama, K. Komaki, Y. Otani, and T. Yoshizawa, "Achromatic axially symmetric wave plate," Opt. Express **20**, 29260–29265 (2012).
19. F. Bouchard, H. Mand, and M. Mirhosseini, "Achromatic orbital angular momentum generator," New J. Phys. **16**, 123006 (2014).
20. N. Radwell, R. D. Hawley, J. B. Gotte, and S. Franke-Arnold, "Achromatic vector vortex beams from a glass cone," Nat. Commun. **7**, 10564 (2016).
21. S. R. Nersisyan, N. V. Tabiryan, D. Mawet, and E. Serabyn, "Improving vector vortex waveplates for high-contrast coronagraphy," Opt. Express **21**, 8205–8213 (2013).
22. C. Oh and M. J. Escuti, "Achromatic diffraction from polarization gratings with high efficiency," Opt. Lett. **33**, 2287–2289 (2008).
23. A. V. Volyar and T. A.Fadeeva, "Generation of singular beams in uniaxial crystals," Opt. Spectrosc. **94**, 235—-244 (2003).
24. C. Fallet and G. Sirat, "Achromatization of conical diffraction: application to the generation of a polychromatic optical vortex," Opt. Lett. **41**, 769–772 (2016).
25. E. Brasselet, Y. Izdebskaya, V. Shvedov, A. S. Desyatnikov, W. Krolikowski, and Y. S. Kivshar, "Dynamics of optical spin-orbit coupling in uniaxial crystals," Opt. Lett. **34**, 1021–1023 (2009).
26. V. Shvedov, W. Krolikowski, A. Volyar, D. N. Neshev, A. S. Desyatnikov, and Y. S. Kivshar, Opt. Express **13**, 7393 – 7398 (2005).
27. E. Brasselet, Y. Izdebskaya, V. Shvedov, A. S. Desyatnikov, W. Krolikowski, and Y. S. Kivshar, Opt. Lett. **34**, 1021 – 1023 (2009).
28. L. Marrucci, C. Manzo, and D. Paparo, "Optical spin-to-orbital angular momentum conversion in inhomogeneous anisotropic media," Phys. Rev. Lett. **96**, 163905 (2006).
29. S. Slussarenko, A. Murauski, T. Du, V. Chigrinov, L. Marrucci, and E. Santamato, "Tunable liquid crystal q-plates with arbitrary topological charge," Opt. Express **19**, 4085–4090 (2011).
30. Y. S. Rumala, G. Milione, T. A. Nguyen, S. Pratavieira, Z. Hossain, D. Nolan, S. Slussarenko, E. Karimi, L. Marrucci, , and R. R. Alfano, "Tunable supercontinuum light vector vortex beam generator using a q-plate," Opt. Lett. **38**, 5083–5086 (2013).
31. K. Yamane, Y. Toda, and R. Morita, "Ultrashort optical-vortex pulse generation in few-cycle regime," Opt. Express **20**, 18986–18993 (2012).
32. M. Beresna, M. Gecevicius, and P. G. Kazansky, "Polarization sensitive

elements fabricated by femtosecond laser nanostructuring of glass," Opt. Mater. Express. **1**, 783–795 (2011).
33. M. Beresna, M. Geceviius, P. G. Kazansky, and T. Gertus, "Radially polarized optical vortex converter created by femtosecond laser nanostructuring of glass," Appl. Phys. Lett. **98**, 201101 (2011).
34. A. Matijosius, P. Stanislovaitis, T. Gertus, and V. Smilgevicius, "Formation of optical vortices with topological charge $|l| = 1$ and $|l| = 1/2$ by use of the s-waveplate," Opt. Commun. **324**, 1–9 (2014).
35. Altechna R&D, "Damage threshold," http://www.altechna.com/download/wop/Operation-Manual-_130701.pdf.
36. L. R. Watkins and M. Derbois, "White-light ellipsometer with geometric phase shifter," Appl. Opt. **51**, 5060–5065 (2012).
37. A. Niv, G. Biener, V. Kleiner, and E. Hasman, "Polychromatic vectorial vortex formed by geometric phase elements," Opt. Lett. **32**, 847–849 (2007).
38. M. Sakamoto, R. Fukumoto, N. Murakami, R. Morita, and K. Oka, "Dispersion reduction in generation of high-order optical vortex using axially symmetric half-wave plates," Opt. Rev. **22**, 174–178 (2015).
39. R. Drevinskas and P. G. Kazansky, "High-performance geometric phase elements in silica glass," APL Photonics **2**, 066104 (2017).
40. M. Gecevicius, M. Beresna, R. Drevinskas, and P. G. Kazansky, "Airy beams generated by ultrafast laser-imprinted space-variant nanostructures in glass," Opt. Lett. **39**, 6791–6794 (2014).
41. M. Reuss, J. Engelhardt, and S. W. Hell, "Birefringent device converts a standard scanning microscope into a sted microscope that also maps molecular orientation," Opt. Express **18**, 1049–1058 (2010).
42. R. Loudon, *The Quantum Theory of Light* (Oxford Science Publications, 2000), 3rd ed.
43. D. M. Palacios, I. D. Maleev, A. S. Marathay, and J. G. A. Swartzlander, Phys. Rev. Lett. **92**, 143905 (2004).
44. G. A. Swartzlander and J. Schmit, Phys. Rev. Lett. **93**, 093901 (2004).
45. A. Matijosius, P. Stanislovaitis, T. Gertus, and V. Smilgevicius, Opt. Comm. **324**, 1 – 9 (2014).
46. V. Denisenko, V. Shvedov, A. S. Desyatnikov, D. N. Neshev, W. Krolikowski, A. Volyar, M. Soskin, and Y. S. Kivshar, Opt. Express **17**, 23374 – 23379 (2009).
47. M. V. Berry, New J. Phys. **4**, 66.1 – 66.14 (2002).